Energy cooperation in quantum thermoelectric systems with multiple electric currents*

Yefeng Liu(刘叶锋)[1], Jincheng Lu(陆金成)[1,†], Rongqian Wang(王荣倩)[1], Chen Wang(王晨)[2], and Jian-Hua Jiang(蒋建华)[1,‡]

[1] School of Physical Science and Technology, Soochow University, Suzhou 215006, China
[2] Department of Physics, Zhejiang Normal University, Jinhua 321004, China

(Received 27 January 2020; revised manuscript received 27 February 2020; accepted manuscript online 9 March 2020)

The energy efficiency and output power of a quantum thermoelectric system with multiple electric currents and only one heat current are studied. The system is connected to the hot heat bath (cold bath) through one terminal (multiple terminals). In such configurations, there are multiple thermoelectric effects coexisting in the system. Using the Landauer–Büttiker formalism, we show that the cooperation between the two thermoelectric effects in the three-terminal thermoelectric systems can lead to markedly improved performance of the heat engine. Such improvement also occurs in four-terminal thermoelectric heat engines with three output electric currents. Cooperative effects in these multi-terminal thermoelectric systems can considerably enlarge the physical parameter region that realizes high energy efficiency and output power. For refrigeration, we find that the energy efficiency can also be substantially improved by exploiting the cooperative effects in multi-terminal thermoelectric systems. All these results reveal a useful approach toward high-performance thermoelectric energy conversion in multi-terminal mesoscopic systems.

Keywords: thermoelectric effect, thermodynamics, cooperative effect

PACS: 05.70.Ln, 84.60.–h, 88.05.De, 88.05.Bc **DOI:** 10.1088/1674-1056/ab7da5

1. Introduction

Thermoelectric phenomena at the nanoscales have attracted broad research interest for their relevance with fundamental physics, material science, and renewable energy.[1–5] Understanding and harnessing thermoelectric transport at the nanoscales may lead to various applications, including heat and energy detectors,[6–10] heat rectifiers,[11–14] refrigerators,[15–19] and energy transduction.[20] Enhancing the energy efficiency of thermoelectric devices is one of the main challenges in the study of thermoelectrics. Tremendous efforts have been devoted to the optimization of mesoscopic heat engines and refrigerators in both theories[21–35] and experiments,[36–43] which may give insight into the search of high-performance macroscopic thermoelectric materials formed by assembling mesoscopic systems.

The performance of thermoelectric materials is characterized by the dimensionless figure of merit (ZT), which is solely determined by the transport coefficients, $ZT = \sigma S^2 T/\kappa$.[44] Here T is the temperature, σ, κ, and S are the electric conductivity, the thermal conductivity, and the Seebeck coefficient, respectively. In linear-responses, the maximum energy efficiency is solely determined by the ZT factor as

$$\eta_{\max} = \eta_{\rm C}\frac{\sqrt{ZT+1}-1}{\sqrt{ZT+1}+1}, \tag{1}$$

where $\eta_{\rm C}$ is the Carnot efficiency.

The conventional approaches toward high-performance thermoelectrics include tuning the electronic and vibrational properties in various ways to increase the ZT and the power density (characterized by the power factor $PF \equiv \sigma S^2$). In most instances, the electric conductivity, the Seebeck coefficient, and the thermal conductivity are correlated, which makes it hard to optimize them independently. Apart from the insight based on Eq. (1), it was recently proposed that in multi-terminal thermoelectric systems, the energy efficiency and output power can be improved through the cooperative effects. The coexistence of multiple thermoelectric effects in those systems enables cooperation between different thermoelectric transport channels, which leads to the enhancement of the thermoelectric performance. In Ref. [45], it was proposed that two coexisting thermoelectric effects induced by the inelastic hopping transport can generate cooperative effects, leading to the enhanced energy efficiency and output power. The generalized thermoelectric figure of merit and power factor for the three-terminal systems which consist of two heat currents and one electric current were introduced as the theoretical framework for the cooperative effect.[45] This study was later extended to three-terminal thermoelectric systems with elastic transport between three electrodes.[46] However, among these studies as well as others, multiple (three or more)

*Project supported by the National Natural Science Foundation of China (Grant Nos. 11675116 and 11704093), the Jiangsu Specially-Appointed Professor Funding, and a Project Funded by the Priority Academic Program Development of Jiangsu Higher Education Institutions (PAPD), China.

†Corresponding author. E-mail: jincheng.lu1993@gmail.com
‡Corresponding author. E-mail: jianhuajiang@suda.edu.cn

heat baths with different temperatures are used, which are difficult to implement in practice.

In this work, we demonstrate that cooperative effects can be exploited to enhance thermoelectric performance even in set-ups with two heat baths. Two prototypes of cooperative thermoelectric devices are illustrated in Fig. 1 where multiple electrodes (with different electrochemical potentials) are mounted onto the two heat baths. The temperatures of the hot and cold baths are kept at $T_{\rm h}$ and $T_{\rm c}$, respectively. Due to the multi-terminal geometry, there are multiple thermoelectric effects coexisting in the systems, described by multiple Seebeck coefficients for thermoelectric transport between various pairs of terminals. By making use of the cooperative effects, the thermoelectric performance can be improved, as compared with the situation where only one of them is involved in the energy conversion. Moreover, such cooperative effects exist in a wide parameter region, leading to the considerably enlarged physical parameter space with high thermoelectric performance. Thus, it becomes less demanding to achieve high-performance thermoelectrics in multi-terminal systems when the cooperative effects are exploited. To demonstrate such effects, three-terminal heat engines and refrigerators as well as four-terminal heat engines are studied in this work.

The main part of this paper is organized as follows. In Section 2, we introduce the three-terminal thermoelectric system and its transport properties, give the expressions for the maximum efficiency and maximum power in the linear-response regime. In Section 3, we show that the cooperative effect can enhance the performance of the three-terminal heat engine in the linear-response regime. In Section 4, we study the cooperative effects in a refrigeration set-up. In Section 5, we compare the optimal efficiency and power of a four-terminal thermoelectric heat engine with those of the three-terminal heat engine. Finally, we conclude our study in Section 6 along with our future outlook.

2. Linear-response thermoelectric transport in a quantum three-terminal heat engine

We consider a nanoscale thermoelectric system consisting of triple quantum dots (QDs) coupled to three electrodes (see Fig. 1). One electrode is mounted onto one heat bath and the others are mounted onto another heat bath. The system can function as a heat engine or a refrigerator depending on the voltage and temperature configurations. In the high-temperature regime, the inter-QD Coulomb interaction can be ignored.[47,48] The intra-QD Coulomb interaction, which is not relevant for the essential physics to be revealed in this work, is also neglected. Each QD is coupled to the nearby reservoir. We employ the indices $1/2/3$ to identify the leads $L/R/P$, respectively.

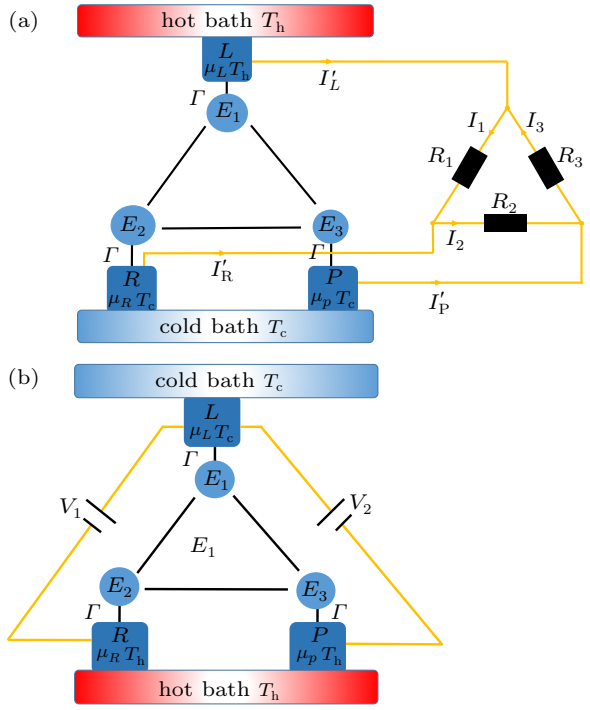

Fig. 1. (a) Schematic figure of a three-terminal triple-QD thermoelectric heat engine. Three quantum dots with a single energy level E_i ($i = L,R,P$) are connected in series to three fermionic reservoirs i. The chemical potential and temperature of the reservoirs are μ_i and T_i, respectively. The constant Γ represents the coupling strength between the quantum dot and electrode. We consider in this set-up that the terminal L is connected to a hot bath and terminals R and P are connected to a cold bath. Besides, the whole thermoelectric system is connected to a circuit with three resistors (denoted as R_i, $i = 1,2,3$). These resistors are respectively connected to three electrodes. I_i represents the current flowing through each resistor. (b) Schematic figure of a three-terminal triple-QD refrigerator, where terminal L is connected to a cold bath and terminals R and P are connected to a hot bath. In this set-up, the terminal L can be cooled.

The system is described by the Hamiltonian[49]

$$\hat{H} = \hat{H}_{\rm QD} + \sum_{i=1,2,3}\sum_{k}\varepsilon_k c_{ik}^{\dagger}c_{ik} + \sum_{i,k}V_k d_i^{\dagger}c_{ik} + {\rm H.c.}, \quad (2)$$

where

$$\hat{H}_{\rm QD} = \sum_{i=1,2,3} E_i d_i^{\dagger}d_i + (t d_{i+1}^{\dagger}d_i + {\rm H.c.}). \quad (3)$$

Here, d_i ($d_i^{\dagger}$) annihilates (creates) an electron in the i-th QD with energy E_i, t is the hopping strength between the QDs, and c_{ik} ($c_{ik}^{\dagger}$) annihilates (creates) an electron in the i-th electrode with energy ε_k.

We take the temperature and the electrochemical potential of reservoir R as a reference, we restrict our study to the linear-response regime. We thus define the flowing thermodynamic "forces"

$$F_{\rm e}^i = \frac{\mu_i - \mu_R}{e}, \quad F_Q^i = \frac{T_i - T_R}{T_R}, \quad (i = L,P), \quad (4)$$

where $e < 0$ is the electron charge. We consider the set-up where the electrode L is connected to the hot bath and the electrodes R and P are connected to the cold bath, i.e., $T_L \equiv T_{\rm h}$ and

$T_R = T_P \equiv T_c$. In this configuration, there is one heat current flowing out of the hot reservoir L which is $I_Q^L = I_Q$. The corresponding force is $F_Q \equiv F_Q^L$. There are two independent electric currents, I_e^L (i.e., the electrical current flowing out of the reservoir L) and I_e^P (i.e., the electrical current flowing out of the reservoir P).

In the linear-response regime, the charge and heat transports are described by the following equation:[50,51]

$$\begin{pmatrix} I_e^L \\ I_e^P \\ I_Q \end{pmatrix} = \begin{pmatrix} M_{11} & M_{12} & M_{13} \\ M_{12} & M_{22} & M_{23} \\ M_{13} & M_{23} & M_{33} \end{pmatrix} \begin{pmatrix} F_e^L \\ F_e^P \\ F_Q \end{pmatrix}, \tag{5}$$

where the charge and heat currents flowing out of the left reservoir can be calculated by the Landauer–Büttiker formalism[52,53]

$$I_e^L = \frac{2e}{h}\int_{-\infty}^{\infty} \mathrm{d}E \sum_i \mathscr{T}_{iL}(E)[f_L(E) - f_i(E)], \tag{6}$$

$$I_Q = \frac{2}{h}\int_{-\infty}^{\infty} \mathrm{d}E \sum_i (E-\mu_L)\mathscr{T}_{iL}(E)[f_L(E) - f_i(E)]. \tag{7}$$

Here $f_i(E) = \{\exp[(E-\mu_i)/k_B T_i] + 1\}^{-1}$ is the Fermi–Dirac distribution function and h is the Planck's constant. The factor of two comes from the spin degeneracy of electrons. $\mathscr{T}_{ij}(E)$ is the transmission probability from terminal j to terminal i[54]

$$\mathscr{T}_{ij} = \mathrm{Tr}[\Gamma_i(E)G(E)\Gamma_j(E)G^{\dagger}(E)], \tag{8}$$

where the (retarded) Green's function is given by $G(E) \equiv [E - H_{QD} - \mathrm{i}\Gamma/2]^{-1}$. The QD–electrode coupling $\Gamma = 2\pi\sum_k |V_{ik}|^2 \delta(\omega - \varepsilon_{ik})$ is assumed to be an energy-independent constant for all three electrodes. Analogous expressions can be written for I_e^P, provided that the index L is substituted by P in Eq. (6). The detailed calculation of Onsager transport coefficients M_{ij} $(i,j = 1,2,3)$ can be found in Appendix A.

The total entropy production accompanying this transport process reads[21]

$$T\dot{\mathscr{S}} = I_e^L F_e^L + I_e^P F_e^P + I_Q F_Q. \tag{9}$$

The second law of thermodynamics, i.e., $\dot{\mathscr{S}} \geq 0$ for arbitrary configurations of thermodynamic forces, imposes the following constraints on the linear-transport properties:

$$\begin{aligned} &M_{11}, M_{22}, M_{33} \geq 0, \quad M_{11}M_{22} \geq M_{12}^2, \\ &M_{11}M_{33} \geq M_{13}^2, \quad M_{22}M_{33} \geq M_{23}^2, \end{aligned} \tag{10}$$

as well as the requirement of non-negativeness of the determinant of the 3×3 transport matrix in Eq. (5).

3. Cooperative thermoelectric effects: A geometric interpretation

In this section, we study the cooperative effects in a thermoelectric engine and elucidate such cooperative effects by a geometric interpretation[45,46]

$$F_e^L = F_e \cos\theta, \quad F_e^P = F_e \sin\theta, \tag{11}$$

where $F_e = \sqrt{(F_e^L)^2 + (F_e^P)^2}$ is the total "magnitude" of electrical affinities. For our further discussion, we define the effective electrical conductance as a function of the parameter θ,[46]

$$G_{\mathrm{eff}}(\theta) = M_{11}\cos^2\theta + 2M_{12}\sin\theta\cos\theta + M_{22}\sin^2\theta. \tag{12}$$

The effective thermoelectric coefficient and the thermal conductance are respectively given by

$$L_{\mathrm{eff}}(\theta) = M_{13}\cos\theta + M_{23}\sin\theta, \quad K = M_{33}, \tag{13}$$

Using the above relations, we can write the figure of merit ZT for a given parameter θ as[55]

$$ZT = \frac{L_{\mathrm{eff}}^2(\theta)}{G_{\mathrm{eff}}(\theta)K - L_{\mathrm{eff}}^2(\theta)}. \tag{14}$$

The energy efficiency of the three-terminal thermoelectric heat engine is defined as[54]

$$\eta = -\frac{W}{I_Q} = -\frac{I_e^L F_e^L + I_e^P F_e^P}{I_Q} \leq \eta_{\max} = \eta_C \frac{\sqrt{ZT+1}-1}{\sqrt{ZT+1}+1}, \tag{15}$$

which is bounded by the Carnot efficiency $\eta_C \equiv (T_h - T_c)/T_h$.

The conditional maximum output power is found as[50]

$$\begin{aligned} W(\theta) &= \frac{1}{4}\frac{L_{\mathrm{eff}}^2(\theta)}{G_{\mathrm{eff}}(\theta)}F_Q^2 \\ &= \frac{(M_{13}\cos\theta + M_{23}\sin\theta)^2}{M_{33}(M_{11}\cos^2\theta + 2M_{12}\sin\theta\cos\theta + M_{22}\sin^2\theta)} W_3, \end{aligned} \tag{16}$$

where we have defined $W_3 = \frac{1}{4}M_{33}F_Q^2$. Here, we call the thermoelectric effect associated with F_e^L as the "L-R thermoelectric effect", while the one associated with F_e^P as the "P-R thermoelectric effect".

When $\theta = 0$ or π, equation (16) gives the L-R thermoelectric efficiency and power

$$\eta_{L-R} = \frac{\sqrt{M_{11}M_{33}} - \sqrt{M_{11}M_{33} - M_{13}^2}}{\sqrt{M_{11}M_{33}} + \sqrt{M_{11}M_{33} - M_{13}^2}}\eta_C, \tag{17a}$$

$$W_{L-R} = \frac{M_{13}^2}{M_{11}M_{33}} W_3. \tag{17b}$$

The P-R thermoelectric efficiency and power are acheived at $\theta = \pi/2$ or $3\pi/2$, which are given by

$$\eta_{P-R} = \frac{\sqrt{M_{22}M_{33}} - \sqrt{M_{33}M_{22} - M_{23}^2}}{\sqrt{M_{22}M_{33}} + \sqrt{M_{33}M_{22} - M_{23}^2}}\eta_C, \tag{18a}$$

$$W_{P-R} = \frac{M_{23}^2}{M_{22}M_{33}} W_3. \tag{18b}$$

In linear-responses, the global maximum energy efficiency and the efficiency at the maximum output power[56–58] of the three-terminal heat engine with the cooperative effects taken into account are respectively given by

$$\eta_{\max} = \frac{1-\sqrt{1-\lambda}}{1+\sqrt{1-\lambda}}\eta_{\rm C}, \tag{19}$$

$$\eta(W_{\max}) = \frac{\lambda}{4-2\lambda}\eta_{\rm C}, \tag{20}$$

It is found that the maximum output power and the output power at the maximum efficiency are

$$W_{\max} = \lambda W_3, \tag{21}$$

$$W(\eta_{\max}) = \lambda\left[1-\left(\frac{\eta_{\max}}{\eta_{\rm C}}\right)^2\right]W_3. \tag{22}$$

Here,

$$\lambda \equiv \frac{M_{13}^2M_{22}+M_{11}M_{23}^2-2M_{12}M_{13}M_{23}}{M_{33}(M_{11}M_{22}-M_{12}^2)} \tag{23}$$

is a dimensionless parameter which is termed as the "degree of coupling".

To illustrate how the two thermoelectric effects cooperate, we plot the energy efficiency η and output power W as functions of the parameter θ in Figs. 2(a) and 2(b). The efficiencies and powers of the *L*-*R* and *P*-*R* thermoelectric effects are also respectively marked with red and blue dots for comparison. It is seen that in the ranges of $0<\theta<\pi/6$ and $\pi<\theta<7\pi/6$, the energy efficiency is greater than both the efficiencies η_{L-R} and η_{P-R} when the *L*-*R* and *P*-*R* thermoelectric effects are considered independently. In the same region of physical parameters, the cooperative output power W is also greater than both the output powers W_{L-R} and W_{P-R}.

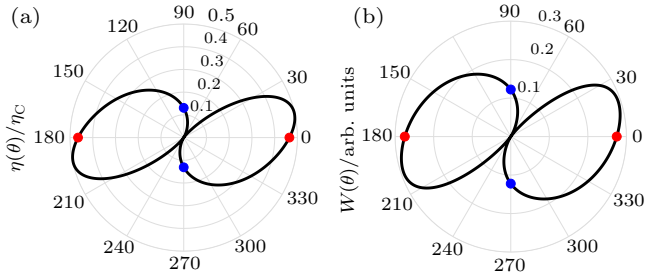

Fig. 2. Polar plots of (a) the efficiency $\eta(\theta)$ in units of Carnot efficiency $\eta_{\rm C}$ [Eq. (15)] and (b) power $W(\theta)$ [Eq. (16)] as a function of the parameter θ. At $\theta=0$ or π, the values of $\eta(\theta)$ and $W(\theta)$ recover those for the *L*-*R* thermoelectric effect (red dots). While at $\theta=\pi/2$ or $3\pi/2$, they go back to the values of the *P*-*R* thermoelectric effect (blue dots). The parameters are $t=-0.2k_{\rm B}T$, $\Gamma=0.5k_{\rm B}T$, $\mu=0$, $E_1=1.0k_{\rm B}T$, $E_2=2.0k_{\rm B}T$, and $E_3=1.0k_{\rm B}T$.

To clarify the enhancement of the thermoelectric performance due to the cooperation effect, we study the maximum efficiency $\eta_{\max}$ and the maximum output power $W_{\max}$ as functions of QD energies E_1 and E_2. It is seen from Figs. 3(a) and 3(c) that $\eta_{\max}$ and $W_{\max}$ are very sensitive to the QDs energies which can be controlled via gate-voltage in experiments.[11] As shown by the hot-spot regions, the optimal values of $\eta_{\max}$ and $W_{\max}$ are achieved when $E_1\approx E_2>1.0k_{\rm B}T$, reaching to $\eta_{\max}\approx 0.6\eta_{\rm C}$. Besides, both the efficiency and power are symmetric around the line of $E_1=E_2$ when $E_3=0$. Figures 3(b) and 3(d) show that the enhancement of the performance is prominent when $E_1\approx 0$. The enhancement factors of the maximum output power $W_{\max}/(W_{L-R},W_{P-R})$ and the maximum efficiency $\eta_{\max}/(\eta_{L-R},\eta_{P-R})$ can reach 10 in a wide range of E_2. It is also noticed that the enhancement factors of both output power and efficiency are always greater than 1. From the above results, we conclude that the cooperative effects can always enhance the performance of three-terminal thermoelectric engines, which opens a pathway toward high-performance thermoelectric energy conversion in multi-terminal thermoelectric systems.

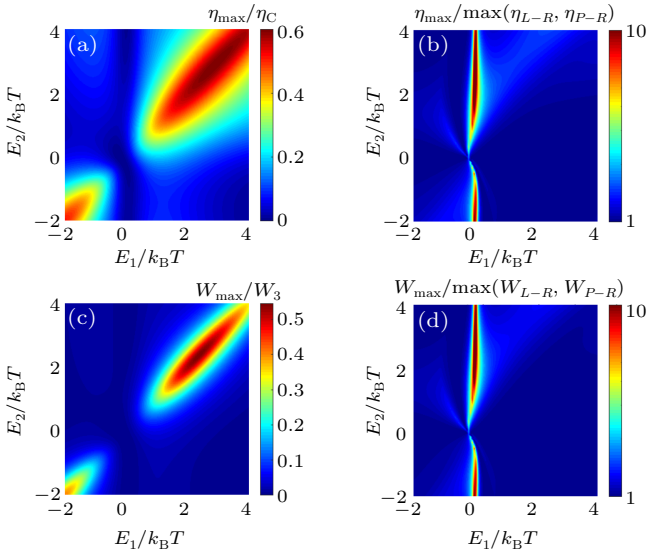

Fig. 3. (a) The maximum efficiency $\eta_{\max}$ in units of Carnot efficiency $\eta_{\rm C}$ [Eq. (19)], (b) the enhancement factor of the efficiency $\eta_{\max}/\max(\eta_{L-R},\eta_{P-R})$, (c) the maximum output power $W_{\max}$ [Eq. (21)], and (d) the enhancement factor of the power $W_{\max}/\max(W_{L-R},W_{P-R})$ as functions of E_1 and E_2. The parameters are $t=-0.2k_{\rm B}T$, $\Gamma=0.5k_{\rm B}T$, $\mu=0$, and $E_3=0$.

We now study the problem of optimizing energy efficiency and output power when the three-terminal thermoelectric heat engine is connected to a resistor circuit. As illustrated in Fig. 1(a), we employ a triangular resistance circuit (with three resistors R_1, R_2, and R_3) to harvest the electric power. The resistances, R_i $(i=1,2,3)$, are tuned to optimize the performance of the three-terminal heat engine. The current–force relation for the triangular resistance circuit is formally written as

$$\boldsymbol{I}'_{\rm e} = \hat{\boldsymbol{M}}^{3\rm T}\boldsymbol{F}_{\rm e} \tag{24}$$

where $\boldsymbol{I}'_{\rm e}=(I'_L,I'_P)^{\rm T}$, I'_L and I'_P are the charge currents flowing out of electrodes *L* and *P*, respectively, into the resistor circuit. The electrical currents flowing through resistors R_i $(i=1,2,3)$

are given by

$$I_1 = \frac{\mu_L - \mu_R}{eR_1} = \frac{F_e^L}{R_1}, \tag{25a}$$

$$I_2 = \frac{\mu_R - \mu_P}{eR_2} = -\frac{F_e^P}{R_2}, \tag{25b}$$

$$I_3 = \frac{\mu_P - \mu_L}{eR_3} = \frac{F_e^P - F_e^L}{R_3}. \tag{25c}$$

According to the Kirchhoff's current law, we obtain

$$\begin{aligned} I_L' - I_1 + I_3 &= 0, \\ I_P' + I_2 - I_3 &= 0. \end{aligned} \tag{26}$$

Using Eqs. (24)–(26), we obtain the expression of $\hat{M}^{3T}$ as

$$\hat{M}^{3T} = \begin{pmatrix} \frac{1}{R_1} + \frac{1}{R_3} & -\frac{1}{R_3} \\ -\frac{1}{R_3} & \frac{1}{R_2} + \frac{1}{R_3} \end{pmatrix}. \tag{27}$$

According to Ref. [59], we find that the maximum power $W_{\max}$ in Eq. (21) is achieved at

$$\hat{M}^{3T} = \begin{pmatrix} M_{11} & M_{12} \\ M_{12} & M_{22} \end{pmatrix}. \tag{28}$$

Besides, the maximum energy efficiency $\eta_{\max}$ in Eq. (19) is achieved at

$$\hat{M}^{3T} = \sqrt{1-\lambda} \begin{pmatrix} M_{11} & M_{12} \\ M_{12} & M_{22} \end{pmatrix}. \tag{29}$$

4. Thermoelectric cooperative effects on a three-terminal refrigerator

The three-terminal device can also operate as a thermoelectric refrigerator by reversing the electrical currents and exchanging the temperatures of the two heat baths.[11,18,50] In this configuration, there are two electrodes mounted on the hot bath, while one electrode mounted on the cold bath which is to be cooled, i.e., $T_{R(P)} = T_h$, $T_L = T_c$, with $T_h > T_c$, as depicted in Fig. 1(b). The consumed electrical power for the cooling is

$$W^{in} = I_e^L F_e^L + I_e^P F_e^P, \tag{30}$$

while the cooling power is I_Q. The efficiency of the refrigerator is

$$\eta^{ref} = \frac{I_Q}{W^{in}} = \frac{I_Q}{I_e^L F_e^L + I_e^P F_e^P} \leq \eta_C. \tag{31}$$

The Carnot efficiency for the refrigerator is given by

$$\eta_C = \frac{T_c}{T_h - T_c}. \tag{32}$$

Using Eq. (5), the cooling heat flux I_Q can be expressed as

$$I_Q = I_{Q,1} + I_{Q,2} + I_{Q,3}, \tag{33}$$

which consists of three parts: the heat current $I_{Q,3} = M_{33}F_Q < 0$ due to the (Fourier) thermal conduction, the cooling heat current $I_{Q,1} = M_{13}F_e^L$ as contributed by the *L*-*R* Peltier effect, and the cooling heat current $I_{Q,2} = M_{23}F_e^P$ as contributed by the *P*-*R* Peltier effect. The cooling is achieved when the sum of the heat currents $I_{Q,1}$ and $I_{Q,2}$ exceeds the thermal conduction current $|I_{Q,3}|$. Combining Eq. (11), the effective heat current can be expressed as a function of the parameter θ,

$$I_Q = M_{13}F_e \cos\theta + M_{23}F_e \sin\theta + M_{33}F_Q. \tag{34}$$

The above equation indicates that $I_{Q,1} = M_{13}F_e\cos\theta$ and $I_{Q,2} = M_{23}F_e\sin\theta$ can be tuned effectively by the parameter θ. When these two currents are of the same sign, i.e., $I_{Q,1} > 0$ and $I_{Q,2} > 0$, they contribute constructively to the cooling. This cooperative effect leads to enhanced cooling power [as shown in Fig. 4(a)] and the energy efficiency [as shown in Fig. 4(b)]. Explicitly, we find that when $0 < \theta < \pi/2$, the two cooling heat currents $I_{Q,1}$ and $I_{Q,2}$ are of the same sign, the cooling power and the energy efficiency are enhanced. In contrast, for $\pi/2 < \theta < 2\pi$, the two cooling heat currents are of opposite signs, the cooling power and the energy efficiency are reduced.

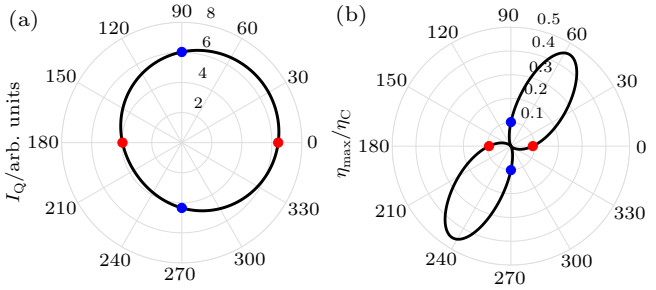

Fig. 4. Polar plots of (a) the effective cooling heat current I_Q and (b) efficiency $\eta_{\max}$ as a function of θ. The red dots represent the *L*-*R* thermoelectric effect, and blue dots represent the *P*-*R* thermoelectric effect. The parameters are $t = 0.2k_BT$, $\Gamma = 0.5k_BT$, $\mu = 0$, $E_1 = 0.2k_BT$, $E_2 = 2.0k_BT$, $E_3 = -2.0k_BT$, and $F_e = F_Q = 1$.

5. The optimal efficiency and power of a four-terminal thermoelectric heat engine

In this section, we study the optimal efficiency and output power of a four-terminal thermoelectric heat engine and compare the optimal performance of the four-terminal thermoelectric heat engine with that of the three-terminal thermoelectric heat engine.[60–64] As shown in Fig. 5, we focus on the situation where the reservoir 1 is connected to the hot bath and the reservoirs 2, 3, and 4 are connected to the cold bath. In this set-up, there are three independent output electric currents I_e^i ($i = 1,2,3$) and only one input heat current I_Q^{4T} flowing out of the hot reservoir 1. In linear-responses, the currents and forces are related to each other through the linear-transport coefficients M_{ij} ($i,j = 1,2,3,4$) as[50]

$$\begin{pmatrix} I_e^1 \\ I_e^2 \\ I_e^3 \\ I_Q^{4T} \end{pmatrix} = \begin{pmatrix} M_{11} & M_{12} & M_{13} & M_{14} \\ M_{12} & M_{22} & M_{23} & M_{24} \\ M_{13} & M_{23} & M_{33} & M_{34} \\ M_{14} & M_{24} & M_{34} & M_{44} \end{pmatrix} \begin{pmatrix} F_e^1 \\ F_e^2 \\ F_e^3 \\ F_Q^{4T} \end{pmatrix}, \tag{35}$$

where I_e^i represents the electric current flowing out of the electrode $i = 1,2,3$. The thermodynamic force corresponding to the electric current I_e^i is $F_e^i = \frac{\mu_i - \mu_4}{e}$ $(i = 1,2,3)$. I_Q^{4T} is the heat current flowing out of the electrode 1 with the corresponding thermodynamic force given by $F_Q^{4T} = \frac{T_1 - T_4}{T_1} = \frac{T_h - T_c}{T_h}$. Detailed calculation of the currents and transport coefficients M_{ij} $(i,j = 1,2,3,4)$ can be found in Appendix B.

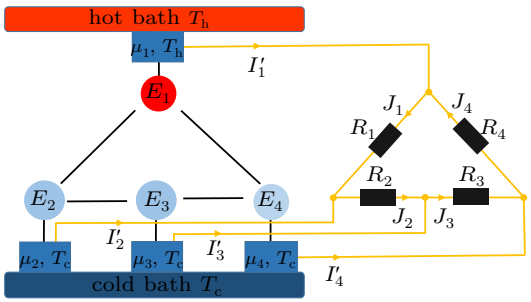

Fig. 5. Schematic figure of a four-terminal thermoelectric heat engine. The QDs system is connected to a resistor circuit. The four resistors (denoted as R_i, $i = 1,2,3,4$) are connected to the four electrodes. The electrochemical potential and the temperature of the electrode i are μ_i and T_i, respectively. J_i $(i = 1,2,3,4)$ represents the current flowing through the resistor R_i.

For a multi-terminal machine, the steady-state heat-to-work conversion efficiency η^{4T} is defined by the ratio between the output power W^{4T} and the heat current I_Q^{4T}, i.e.,

$$\eta^{4T} = -\frac{W^{4T}}{I_Q^{4T}} \leq \eta_C, \tag{36}$$

$$W^{4T} = \sum_{i=1,2,3} I_e^i F_e^i, \tag{37}$$

$$\eta_C = F_Q^{4T} = \frac{T_h - T_c}{T_h}. \tag{38}$$

Here, $\eta^{4T} \leq \eta_C$ is dictated by the second-law of thermodynamics, i.e., the total entropy production rate $\sum_{i=1,2,3} I_e^i F_e^i + I_Q^{4T} F_Q^{4T} \geq 0$. The maximum energy efficiency and the efficiency at the maximum output power are respectively found to be

$$\eta_{max}^{4T} = \frac{1 - \sqrt{1-\Lambda}}{1 + \sqrt{1-\Lambda}} \eta_C, \tag{39}$$

$$\eta^{4T}(W_{max}) = \frac{\Lambda}{4 - 2\Lambda} \eta_C. \tag{40}$$

Besides, the maximum output power and the output power at the maximum efficiency are respectively found to be

$$W_{max}^{4T} = \Lambda W_4, \quad W_4 = \frac{1}{4} M_{44} F_Q^2, \tag{41}$$

$$W^{4T}(\eta_{max}) = \Lambda \left[1 - \left(\frac{\eta_{max}}{\eta_C} \right)^2 \right] W_4. \tag{42}$$

Here,

$$\Lambda = \hat{M}_{Qe} \hat{M}_{ee}^{-1} \hat{M}_{eQ} M_{QQ}^{-1} \tag{43}$$

is the so-called degree of coupling. $\hat{M}_{ee}$ denotes the 3×3 charge conductivity tensor. $\hat{M}_{eQ}$ and $\hat{M}_{Qe}$ are the 3×1 and 1×3 matrices, respectively, describing the Seebeck and Peltier effects. M_{QQ} represents the heat conductivity.

We first examine the optimal efficiency and output power of the four-terminal heat engine and then compare them with those of the three-terminal heat engine. As shown in Fig. 6, we plot the maximum efficiency η_{max}^{4T} and the efficiency at the maximum output power $\eta^{4T}(W_{max})$ as functions of the QD energy E_4. From Figs. 6(a) and 6(c), we find that both of η_{max}^{4T} and $\eta^{4T}(W_{max})$ achieve their maximum values at $E_4 \approx 1.2 k_B T$. Especially when $E_2 = -2k_B T$, the maximum efficiency η_{max}^{4T} is found to be $0.4\eta_C$. As shown in Figs. 6(b) and 6(d), both of the maximum efficiency and the efficiency at the maximum power of the four-terminal heat engine are greater than those of the three-terminal heat engine in the range of $0.2k_B T < E_4 < 4k_B T$. These comparisons illustrate that the heat engine with multiple output electrical currents offers accesses to better performance.

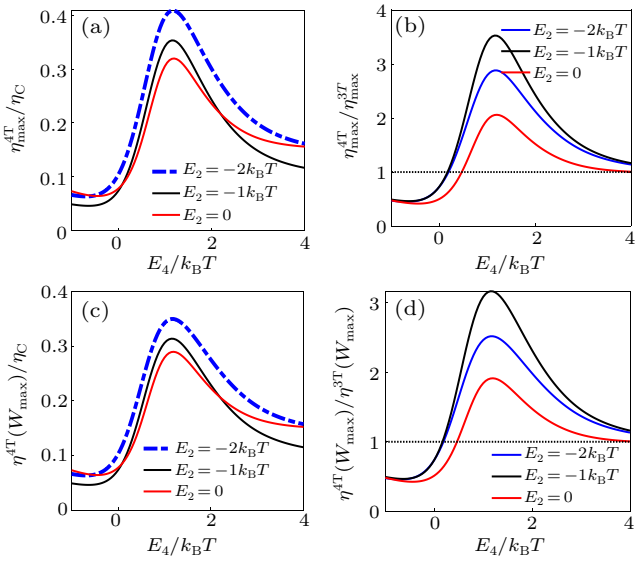

Fig. 6. (a) The maximum efficiency η_{max}^{4T} and (c) the efficiency at the maximum output power $\eta^{4T}(W_{max})$ for four-terminal thermoelectric devices as functions of the QD energy E_4 for different energies E_2. (b) and (d) present the ratio of the energy efficiency between the four-terminal and the three-terminal heat engines under the maximum energy efficiency and the maximum power conditions, respectively. The other parameters are $E_1 = 1.0 k_B T$, $E_3 = 3.0 k_B T$, $\mu = 0$, and $t = -0.2 k_B T$.

In order to verify the above results, we further study the maximum energy efficiency, the energy efficiency at the maximum power, the maximum output power, and the output power at the maximum efficiency as functions of QD energies E_3 and E_4. Both of the efficiencies and powers are symmetric around the line of $E_3 = E_4$. The improvements are especially pronounced when $E_3 > 1k_B T$ and $E_4 > 1k_B T$ with the optimal energy efficiency of the four-terminal thermoelectric heat engine reaching to $0.5\eta_C$. Figure 8 shows the comparisons of the optimal performances between the four-terminal and

three-terminal set-ups, it is found that the energy efficiency and output power are considerably enhanced by using the four-terminal set-up, particularly when $0.5k_{\rm B}T < E_4 < 1.5k_{\rm B}T$, $E_3 < 0$, as well as $E_3 > 2k_{\rm B}T$.

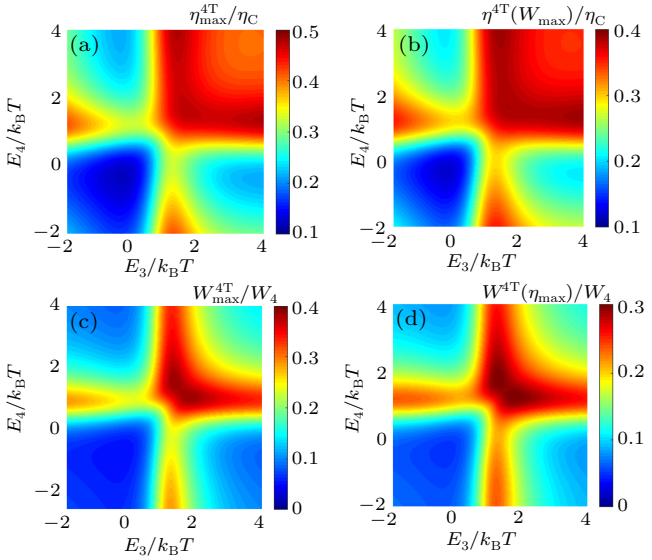

Fig. 7. The optimal performances of the four-terminal heat engine for various QD energies E_3 and E_4. (a) The maximum efficiency [Eq. (39)], (b) the efficiency at the maximum output power [Eq. (40)], (c) the maximum output power [Eq. (41)], and (d) the output power at the maximum efficiency [Eq. (42)]. The other parameters are $t = -0.2k_{\rm B}T$, $\mu = 0$, $E_1 = 1.0k_{\rm B}T$, and $E_2 = 2.0k_{\rm B}T$.

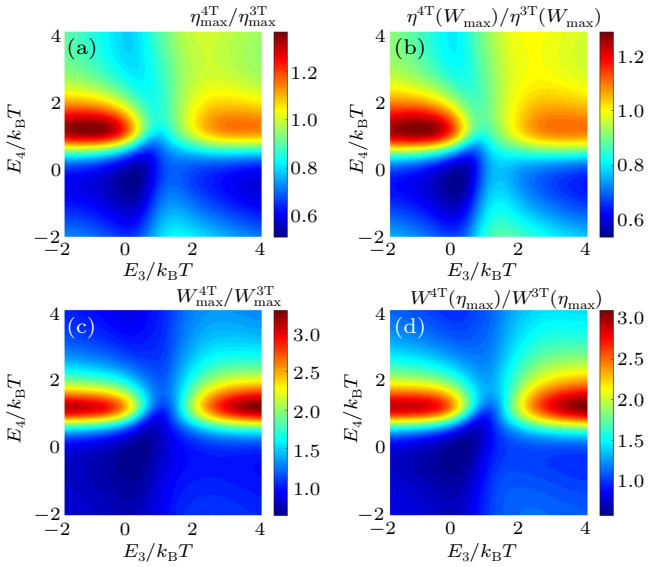

Fig. 8. Comparisons of the optimal performances between the four-terminal and three-terminal heat engines for various QD energies E_3 and E_4. (a) The maximum efficiency, (b) the efficiency at the maximum output power, (c) the maximum output power, and (d) the output power at the maximum efficiency. The other parameters are $t = -0.2k_{\rm B}T$, $\mu = 0$, $E_1 = 1.0k_{\rm B}T$, and $E_2 = 2.0k_{\rm B}T$.

Finally, we come to the realistic situations where the four-terminal heat engine is connected to a resistor circuit. The thermoelectric energy is used by the resistor network, as shown in Fig. 5. The relation between the currents and forces of the resistor circuit can be expressed by the Onsager transport matrix $\hat{M}^{4T}$

$$\boldsymbol{I}_{\rm e}^{4T} = \hat{\boldsymbol{M}}^{4T}\boldsymbol{F}_{\rm e}^{4T}, \tag{44}$$

where $\boldsymbol{I}'_{\rm e} = (I'_1, I'_2, I'_3, I'_4)^{\rm T}$ and I'_i $(i = 1,2,3,4)$ is the electric current flowing out of electrode i into the resistor circuit. $\boldsymbol{F}_{\rm e}^{4T} = (F_{\rm e}^1, F_{\rm e}^2, F_{\rm e}^3, F_{\rm e}^4)^{\rm T}$ is the corresponding thermodynamic force. The electric currents J_i flowing through the resistors R_i $(i = 1,2,3,4)$ are given by

$$\begin{aligned} J_1 &= \frac{\mu_1 - \mu_2}{eR_1} = \frac{F_{\rm e}^1 - F_{\rm e}^2}{R_1}, \\ J_2 &= \frac{\mu_2 - \mu_3}{eR_2} = \frac{F_{\rm e}^2 - F_{\rm e}^3}{R_2}, \\ J_3 &= \frac{\mu_3 - \mu_4}{eR_3} = \frac{F_{\rm e}^3}{R_3}, \\ J_4 &= \frac{\mu_4 - \mu_1}{eR_4} = -\frac{F_{\rm e}^1}{R_4}. \end{aligned} \tag{45}$$

According to the Kirchhoff's current law for the resistor circuit, we have

$$\begin{aligned} I'_1 - J_1 + J_4 &= 0, \\ I'_2 + J_1 - J_2 &= 0, \\ I'_3 + J_2 - J_3 &= 0, \\ I'_4 + J_3 - J_4 &= 0. \end{aligned} \tag{46}$$

Combining Eqs. (44)–(46), the expression of $\hat{M}^{4T}$ is found to be

$$\hat{M}^{4T} = \begin{pmatrix} \frac{1}{R_1} + \frac{1}{R_4} & -\frac{1}{R_1} & 0 \\ -\frac{1}{R_1} & \frac{1}{R_1} + \frac{1}{R_2} & -\frac{1}{R_2} \\ 0 & -\frac{1}{R_2} & \frac{1}{R_2} + \frac{1}{R_3} \end{pmatrix}. \tag{47}$$

In addition, the Kirchhoff's current law for the electrodes requires that

$$\boldsymbol{J} + \boldsymbol{I}_e^{4T} = 0. \tag{48}$$

Then we obtain

$$\boldsymbol{F}_{\rm e}^{4T} = -(\hat{\boldsymbol{M}}_{\rm ee} + \hat{\boldsymbol{M}}^{4T})^{-1}\hat{\boldsymbol{M}}_{Q\rm e}\boldsymbol{F}_Q^{4T}. \tag{49}$$

The electric power consumed by the resistor circuit is given by

$$\begin{aligned} W^{4T} &= -(\boldsymbol{F}_{\rm e}^{4T})^{\rm T}\hat{\boldsymbol{M}}^{4T}\boldsymbol{F}_{\rm e}^{4T} \\ &= -\hat{\boldsymbol{M}}_{Q\rm e}(\hat{\boldsymbol{M}}_{\rm ee}+\hat{\boldsymbol{M}}^{4T})^{-1}\hat{\boldsymbol{M}}^{4T}(\hat{\boldsymbol{M}}_{\rm ee}+\hat{\boldsymbol{M}}^{4T})^{-1}\hat{\boldsymbol{M}}_{Q\rm e}(\boldsymbol{F}_Q^{4T})^2. \end{aligned} \tag{50}$$

And the heat current is given by

$$I_Q^{4T} = [-\hat{\boldsymbol{M}}_{\rm eQ}(\hat{\boldsymbol{M}}_{\rm ee} + \hat{\boldsymbol{M}}^{4T})^{-1}\hat{\boldsymbol{M}}_{Q\rm e} + \boldsymbol{M}_{QQ}]\boldsymbol{F}_Q^{4T}. \tag{51}$$

The energy efficiency of the four-terminal heat engine is then defined as $\eta^{4T} = W^{4T}/I_Q^{4T}$. Through the modification of $\hat{M}^{4T}$, the maximum output power is achieved at

$$\hat{M}^{4T} = \hat{M}_{\rm ee}, \tag{52}$$

and the maximum energy efficiency is obtained at

$$\hat{M}^{4T} = \sqrt{1-\Lambda}\,\hat{M}_{\rm ee}, \tag{53}$$

It is noticed that the above formulas of the optimal energy efficiency and output power are consistent with Eqs. (39) and (41).

6. Conclusion

In this work, we show that cooperative effects can be a useful way to improve the energy efficiency and output power of the multi-terminal quantum-dot thermoelectric heat engines with multiple output electric currents. Each pair of terminals (including a hot terminal and a cold terminal) yields a thermoelectric effect. The cooperation between the coexisting multiple thermoelectric effects leads to improved thermoelectric performance. Through the calculation of the thermoelectric transport coefficients using the Landauer–Büttiker formalism, we find that both the efficiency and power can be considerably improved by the cooperative thermoelectric effect, as compared with that using each thermoelectric effect independently. Such improvements are as effective for good thermoelectrics as that for bad thermoelectrics. Therefore, the region of physical parameters with high thermoelectric performance is considerably increased by the thermoelectric effects. By comparing the thermoelectric performance of four-terminal and three-terminal thermoelectric engines, we find that more output electric currents can further improve the performance of quantum heat engines in a certain range of parameters. Our results offer useful guidelines in the understanding of optimal behaviors of the multiple-terminal heat engine in the linear response regime. Nonlinear effects, which may yield interesting effects, deserve future studies.

Appendix A: Calculation of the Onsager transport linear-response coefficients for the three-terminal model

For a three-terminal configuration, as in previous sections, the Onsager transport's coefficients are obtained from the linear expansion of the electronic currents $I^i_{\rm e}$ and heat currents I^i_Q $(i=L,P)$ given by Eqs. (6) and (7). The Onsager transport coefficients M_{ij} can be written in terms of the transmission function $\mathscr{T}_{ij}(E), i,j\in\{L,R,P\}$ as

$$M_{11}=\frac{2e^2}{hk_{\rm B}T}\int_{-\infty}^{\infty}{\rm d}E\sum_{j\neq L}\mathscr{T}_{Lj}(E)F(E), \tag{A1}$$

$$M_{12}=-\frac{2e^2}{hk_{\rm B}T}\int_{-\infty}^{\infty}{\rm d}E\,\mathscr{T}_{LP}(E)F(E), \tag{A2}$$

$$M_{13}=\frac{2e}{hk_{\rm B}T}\int_{-\infty}^{\infty}{\rm d}E(E-\mu)\sum_{j\neq L}\mathscr{T}_{Lj}(E)F(E), \tag{A3}$$

$$M_{22}=\frac{2e^2}{hk_{\rm B}T}\int_{-\infty}^{\infty}{\rm d}E\sum_{j\neq P}\mathscr{T}_{Pj}(E)F(E), \tag{A4}$$

$$M_{23}=-\frac{2e}{hk_{\rm B}T}\int_{-\infty}^{\infty}{\rm d}E(E-\mu)\mathscr{T}_{PL}(E)F(E), \tag{A5}$$

$$M_{33}=\frac{2}{hk_{\rm B}T}\int_{-\infty}^{\infty}{\rm d}E(E-\mu)^2\sum_{j\neq L}\mathscr{T}_{Lj}(E)F(E), \tag{A6}$$

where $F(E)\equiv\{4\cosh^2[(E-\mu)/k_{\rm B}T]\}^{-1}$.

Appendix B: Calculations of the currents and the linear-response coefficients for the four-terminal system

The system Hamiltonian for the four-terminal heat engine reads

$$\hat{H}_{\rm QD}=\sum_{i=1,2,3,4}E_i d_i^{\dagger}d_i. \tag{B1}$$

The transmission probability is given by

$$\mathscr{T}_{ij}={\rm Tr}[\Gamma_i(E)G(E)\Gamma_j(E)G^{\dagger}(E)], \tag{B2}$$

where the (retarded) system Green function $G(E)\equiv[E-H_{\rm QD}-{\rm i}\Gamma/2]^{-1}$, the dot–lead coupling Γ_i is assumed to be a constant for all three electrodes.

The charge and heat currents flowing out of the left reservoir are given by

$$I^i_{\rm e}=\frac{2e}{h}\int_{-\infty}^{\infty}{\rm d}E\sum_{i\neq j}\mathscr{T}_{ij}(E)[f_j(E)-f_i(E)], \tag{B3}$$

$$I_Q=\frac{2}{h}\int_{-\infty}^{\infty}{\rm d}E(E-\mu_1)\sum_{j}\mathscr{T}_{j1}(E)[f_1(E)-f_j(E)]. \tag{B4}$$

The Onsager transport coefficients M_{ij} can be written in terms of the transmission function $\mathscr{T}_{ij}(E)$ as

$$M_{11}=\frac{2e^2}{hk_{\rm B}T}\int_{-\infty}^{\infty}{\rm d}E\sum_{j\neq 1}\mathscr{T}_{1j}(E)F(E), \tag{B5}$$

$$M_{12}=-\frac{2e^2}{hk_{\rm B}T}\int_{-\infty}^{\infty}{\rm d}E\,\mathscr{T}_{12}(E)F(E), \tag{B6}$$

$$M_{13}=-\frac{2e^2}{hk_{\rm B}T}\int_{-\infty}^{\infty}{\rm d}E\,\mathscr{T}_{13}(E)F(E), \tag{B7}$$

$$M_{14}=\frac{2e}{hk_{\rm B}T}\int_{-\infty}^{\infty}{\rm d}E\sum_{j\neq 1}(E-\mu)\mathscr{T}_{1j}(E)F(E); \tag{B8}$$

$$M_{22}=\frac{2e^2}{hk_{\rm B}T}\int_{-\infty}^{\infty}{\rm d}E\sum_{j\neq 2}\mathscr{T}_{2j}(E)F(E), \tag{B9}$$

$$M_{23}=-\frac{2e^2}{hk_{\rm B}T}\int_{-\infty}^{\infty}{\rm d}E\,\mathscr{T}_{23}(E)F(E), \tag{B10}$$

$$M_{24}=\frac{2e}{hk_{\rm B}T}\int_{-\infty}^{\infty}{\rm d}E(E-\mu)\mathscr{T}_{21}(E)F(E); \tag{B11}$$

$$M_{33}=\frac{2e^2}{hk_{\rm B}T}\int_{-\infty}^{\infty}{\rm d}E\sum_{j\neq 3}\mathscr{T}_{3j}(E)F(E), \tag{B12}$$

$$M_{34}=-\frac{2e}{hk_{\rm B}T}\int_{-\infty}^{\infty}{\rm d}E(E-\mu)\mathscr{T}_{31}(E)F(E); \tag{B13}$$

$$M_{44}=\frac{2}{hk_{\rm B}T}\int_{-\infty}^{\infty}{\rm d}E\sum_{j\neq 1}(E-\mu)^2\sum_{j\neq 1}\mathscr{T}_{1j}(E)F(E), \tag{B14}$$

where $F(E)\equiv\{4\cosh^2[(E-\mu)/k_{\rm B}T]\}^{-1}$.

References

[1] Dubi Y and Ventra M Di 2011 *Rev. Mod. Phys.* **83** 131

[2] Sothmann B, Sánchez R and Jordan A N 2015 *Nanotechnology* **26** 032001

[3] Jiang J H and Imry Y 2016 *C. R. Phys.* **17** 1047

[4] Thierschmann H, and Sánchez R, Sothmann B, Buhmann H and Molenkamp L W, 2016 *C. R. Phys.* **17** 1109
[5] Benenti G, Casati G, Saito K and Whitney R S 2017 *Phys. Rep.* **694** 1
[6] Sánchez D and Serra L 2011 *Phys. Rev. B* **84** 201307
[7] Sothmann B, Sánchez R, Jordan A N and Büttiker M 2013 *New J. Phys.* **15** 095021
[8] Jiang J H, Entin-Wohlman O and Imry Y 2013 *Phys. Rev. B* **87** 205420
[9] Jiang J H, Entin-Wohlman O and Imry Y 2013 *New J. Phys.* **15** 075021
[10] Zhang Y, Zhang X, Ye Z, Lin G and Chen J 2017 *Appl. Phys. Lett.* **110** 153501
[11] Jiang J H, Kulkarni M, Segal D and Imry Y 2015 *Phys. Rev. B* **92** 045309
[12] Lu J, Wang R, Ren J, Kulkarni M and Jiang J H 2019 *Phys. Rev. B* **99** 035129
[13] Goury D and Sánchez R 2019 *Appl. Phys. Lett.* **115** 092601
[14] Wang C, Xu D, Liu H and Gao X 2019 *Phys. Rev. E* **99** 042102
[15] Wang R, Lu J, Wang C and Jiang J H 2018 *Sci. Rep.* **8** 2607
[16] Mani A and Benjamin C 2018 *Phys. Rev. E* **97** 022114
[17] Mani A and Benjamin C 2019 *J. Phys. Chem. C* **123** 22858-22864
[18] Sánchez D, Sánchez R, López R and Sothmann B 2019 *Phys. Rev. B* **99** 245304
[19] Zhang Y, Guo J and Chen J 2020 *Physica E* **118** 113874
[20] Simine L and Segal D 2012 *Phys. Chem. Chem. Phys.* **14** 13820
[21] Entin-Wohlman O, Imry Y and Aharony A 2010 *Phys. Rev. B* **82** 115314
[22] Sánchez R and Büttiker M 2011 *Phys. Rev. B* **83** 085428
[23] Jiang J H, Entin-Wohlman O and Imry Y 2012 *Phys. Rev. B* **85** 075412
[24] Whitney R S 2014 *Phys. Rev. B* **112** 130601
[25] Entin-Wohlman O, Jiang J H and Imry Y 2014 *Phys. Rev. E* **89** 012123
[26] Mazza F, Valentini S, Bosisio R, Benenti G, Giovannetti V, Fazio R and Taddei F 2015 *Phys. Rev. B* **91** 245435
[27] Sánchez R, Sothmann B and Jordan A N 2015 *Phys. Rev. Lett.* **114** 146801
[28] Entin-Wohlman O, Imry Y and Aharony A 2015 *Phys. Rev. B* **91** 054302
[29] Agarwalla B K, Jiang J H and Segal D 2015 *Phys. Rev. B* **92** 245418
[30] Yamamoto K, Entin-Wohlman O, and Aharony A and Hatano N 2016 *Phys. Rev. B* **94** 121402
[31] Shiraishi N, Saito K and Tasaki H, 2016 *Phys. Rev. Lett.* **117** 190601
[32] Mani A and Benjamin C 2017 *Phys. Rev. E* **96** 032118
[33] Agarwalla B K, Jiang J H and Segal D 2017 *Phys. Rev. B* **96** 104304
[34] Jiang J H and Imry Y 2018 *Phys. Rev. B* **97** 125422
[35] Hussein R, Governale M, Kohler S, Belzig W, Giazotto F and Braggio A 2019 *Phys. Rev. B* **99** 075429
[36] Hwang S Y, Sánchez D, Lee M and López R 2013 *New J. Phys.* **15** 105012
[37] Matthews J, Battista F, Sánchez D, Samuelsson P and Linke H 2014 *Phys. Rev. B* **90** 165428
[38] Thierschmann H, Sánchez R, Sothmann B, Arnold F, Heyn C, Hansen W, Buhmann H and Molenkamp L W 2014 *Nat. Nanotech.* **10** 854
[39] Cui L, Miao R, Wang K, Thompson D, Zotti L A, Cuevas J C, Meyhofer E and Reddy P 2018 *Nat. Nanotech.* **13** 122
[40] Josefsson M, Svilans A, Burke A M, Hoffmann E A, Fahlvik S, Thelander C, Leijnse M and Linke H 2018 *Nat. Nanotech.* **13** 920
[41] Jaliel G, Puddy R K, Sánchez R, Jordan A N, Sothmann B, Farrer I, Griffiths J P, Ritchie D A and Smith C G 2019 *Phys. Rev. Lett.* **123** 117701
[42] Josefsson M, Svilans A, Linke H and Leijnse M 2019 *Phys. Rev. B* **99** 235432
[43] Prete D, Erdman P A, Demontis V, Zannier V, Ercolani D, Sorba L, Beltram F, Rossella F, Taddei F and Roddaro S 2019 *Nano Lett.* **19** 3033
[44] Mahan G D and Sofo J O 1996 *Proc. Natl. Acad. Sci. USA* **93** 7436
[45] Jiang J H 2014 *J. Appl. Phys.* **116** 194303
[46] Lu J, Wang R, Liu Y and Jiang J H 2017 *J. Appl. Phys.* **122** 044301
[47] Saito K, Benenti G, Casati G and Prosen T 2011 *Phys. Rev. B* **84** 201306
[48] Büttiker M 1988 *IBM J. Res. Dev.* **32** 63
[49] Jiang J H, Agarwalla B K and Segal D 2015 *Phys. Rev. Lett.* **115** 040601
[50] Jiang J H 2014 *Phys. Rev. E* **90** 042126
[51] Jiang J H and Imry Y 2017 *Phys. Rev. Applied* **7** 064001
[52] Sivan U and Imry Y 1986 *Phys. Rev. B* **33** 551
[53] Butcher P N 1990 *J. Phys.: Condens. Matter* **2** 4869
[54] Mazza F, Bosisio R, Benenti G, Giovannetti V, Fazio R and Taddei F 2015 *New J. Phys.* **16** 085001
[55] Benenti G, Saito K and Casati G 2011 *Phys. Rev. Lett.* **106** 230602
[56] Van den Broeck C 2005 *Phys. Rev. Lett.* **95** 190602
[57] Golubeva N and Imparato A 2012 *Phys. Rev. Lett.* **109** 190602
[58] Proesmans K, Cleuren B and Van den Broeck C 2016 *Phys. Rev. Lett.* **116** 220601
[59] Lu J, Liu Y, Wang R, Wang C and Jiang J H 2019 *Phys. Rev. B* **100** 115438
[60] Büttiker M 1986 *Phys. Rev. Lett.* **57** 1761
[61] Hofer P P and Sothmann B 2015 *Phys. Rev. B* **91** 195406
[62] Brandner K and Seifert U 2013 *New J. Phys.* **15** 105003
[63] Sánchez R, Sothmann B and Jordan A N 2016 *Physica E* **75** 86
[64] Brandner K, Hanazato T and Saito K 2018 *Phys. Rev. Lett.* **120** 090601